

## Supplemental information for: “Stability and synthesis across barium tin sulfide material space”

Rachel Woods-Robinson, Kristin A. Persson and Andriy Zakutayev

(Dated: October 13, 2023)

### S1. SCAN PHASE DIAGRAMS

In Figure S1, we have added data from r2SCAN newly available from Materials Project as a point of comparison. This does not substantially change the phase diagram. Note that some materials are not yet available in r2SCAN (right panel), however if we adopt the “mixed phase diagram” methodology of Kingsbury et al.,[1] we can also construct a mixed r2SCAN-GGA phase diagram (center panel), and this too is qualitatively similar. We expect that this agreement is due to the empirical correction scheme of Wang et al.,[2] applied to the GGA phase diagram helps to fix some known issues in GGA with sulphides, which r2SCAN handles without empirical correction. The inclusion of a second method gives us increased confidence in our results, even if in this case it ended up not being necessary. We have retained the GGA+U functional for the SISSO analysis in the manuscript, since Bartel et al. benchmarked this method with GGA+U rather than SCAN.[3]

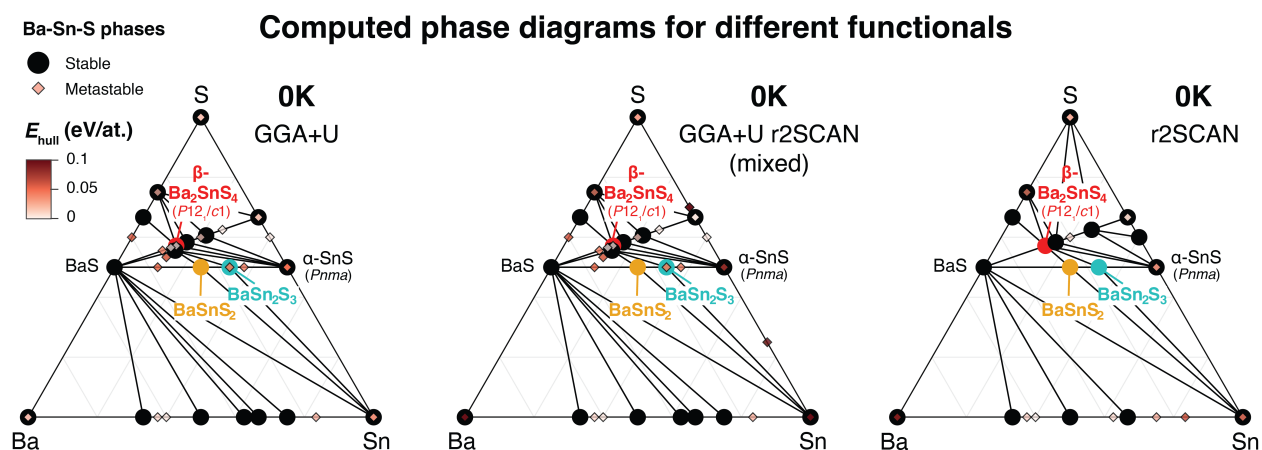


Figure S1: Comparison of GGA+U phase diagram to r2SCAN and r2SCAN mixing.

## S2. FREE ENERGY TERMS FROM SISSO

The SISSO temperature-dependent free energy framework was proposed by Bartel et al.[3] and has been implemented in pymatgen for use in this paper. Since in SISSO the analytical form of free energy  $G(T)$  is known explicitly, here we assess the contributions to free energy by each term of the SISSO equation. Five terms are defined and implemented for a given crystal structure as follows.

1. **Enthalpy term**  $G_{\text{enthalpy}}$ , in which  $H_0$  is the enthalpy of formation at 0K and  $N$  is number of atoms in the unit cell:

$$G_{\text{enthalpy}} = N\Delta H_0 \quad (\text{S1})$$

2. **Volume term**  $G_{\text{volume}}$ , dependent on volume ( $V$ ) and temperature ( $T$ ):

$$G_{\text{volume}}(N, V, T) = -2.48 \times 10^{-4} NT \log(V) \quad (\text{S2})$$

3. **Mass term**  $G_{\text{mass}}$  (or density term), dependent on reduced mass ( $m$ ) divided by  $V$ , as well as  $T$ :

$$G_{\text{mass}}(N, m, V, T) = -8.94 \times 10^{-5} NT(m/V) \quad (\text{S3})$$

4. **Temperature term**  $G_{\text{temp}}$ , dependent on  $T$  and a machine-learned constant.

$$G_{\text{temp}}(N, T) = (0.181 \log(T) - 0.882)N \quad (\text{S4})$$

5. **Elemental Gibbs term**  $G_{\text{elem}}$ , dependent Gibbs free energy of individual elements  $G_i$  weighted by composition ( $c$ ).

$$G_{\text{elem}}(c) = \sum_{i,c} cG_i \quad (\text{S5})$$

**Table S1:** Material-dependent inputs for the SISSO formulation of free energy for materials in this study:  
number of sites, volume, reduced mass.

MPID	Formula	Space group	Sn/ (Ba+Sn)	S/ (Ba+Sn)	# sites ( $N$ )	Volume ( $V$ )	Reduced mass ( $m$ )	$E_{\text{hull}}^{0\text{K}}$ (eV/at.)	$E_{\text{hull}}^{1500\text{K}}$ (eV/at.)
mp-1500	BaS	$Fm\bar{3}m$	0	1	2	33.65	26	0	0
mp-1195594	Ba <sub>8</sub> Sn <sub>4</sub> S <sub>15</sub>	$Pca2_1$	0.33	1.25	216	30.1	34.1	0	0.009
mp-540689	Ba <sub>2</sub> SnS <sub>4</sub>	$Pna2_1$	0.33	1.33	56	31.11	33.8	0.005	0
mp-541832	Ba <sub>2</sub> SnS <sub>4</sub>	$P12_1/c1$	0.33	1.33	28	29.98	33.8	0	0.003
mp-12181	BaSnS <sub>2</sub>	$P2_1/c$	0.5	1	16	30.67	35.13	0	0.09
mp-1183370	BaSnS <sub>3</sub>	$Pnma$	0.5	1.5	20	25.36	33.23	0.016	0.066
mp-27802	BaSn <sub>2</sub> S <sub>3</sub>	$P2_1/m$	0.67	1	36	28.1	35.1	0	0.165
mp-2231	SnS	$Pnma$	1	1	8	25.55	25.25	0	0.353
mp-554134	SnS	$Aem2$	1	1	4	97.6	25.25	0.048	0

Therefore, the total temperature-dependent SISSO energy  $\Delta G_{\text{SISSO}}$  is then:

$$\Delta G_{\text{SISSO}}(N, c, m, V, T) = G_{\text{enthalpy}}(T) + G_{\text{volume}}(N, V, T) + G_{\text{mass}}(N, m, V, T) + G_{\text{temp}}(N, T) + G_{\text{elem}}(c) \quad (\text{S6})$$

The variables within these equations —  $V$ ,  $m$ ,  $N$  — are tabulated in Table S1, alongside their  $E_{\text{hull}}^{0\text{K}}$  and  $E_{\text{hull}}^{1500\text{K}}$  values as reported in the manuscript.

In Figure S2,  $\Delta G_{\text{SISSO}}$  is plotted for each material of interest for temperatures of 0K, 500K, 1000K, and 1500K.

Another way to plot this data, just looking at the highest temperature of 1500 K, is shown in Figure S3. Comparing the two Ba<sub>2</sub>SnS<sub>4</sub> phases (with BaSnS<sub>2</sub> plotted for reference) shows that the biggest contributor to the phase change between the Ba<sub>2</sub>SnS<sub>4</sub> phases is the volume term,  $G_{\text{volume}}$ . Similarly, the SnS phase change and instability of  $Pnma$  phase with increased temperature is also likely due to volume. Therefore, the dominant effect leading to the temperature-dependent instabilities in the SISSO model is volume reduction. This is likely the case for BaSnS<sub>2</sub> as well, but since it is the only polymorph explored we cannot conduct a comparison at fixed composition and therefore cannot conclude this definitively.



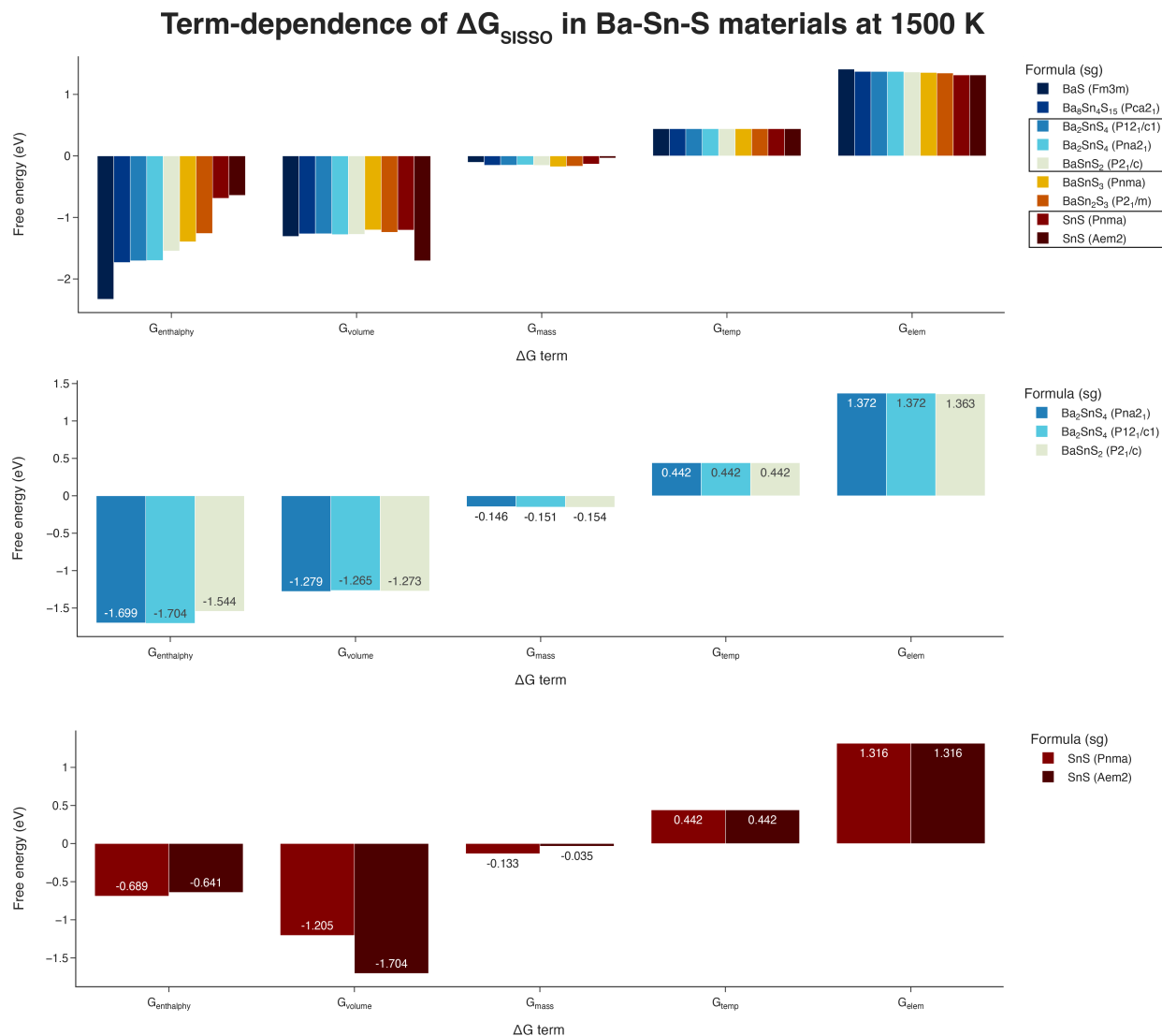


**Figure S3:** Term-dependence of  $G_{\text{SISSO}}$  at 1500K (top), with a comparison of Ba<sub>2</sub>SnS<sub>4</sub> and BaSnS<sub>2</sub> phases (middle) and comparison of SnS phases (bottom).

### S3. POURBAIX MOISTURE SENSITIVITY

Instability to moisture and air are common in many sulfides and other chalcogenides. One well-known example is pyrite (FeS<sub>2</sub>), which is thermodynamically metastable but is highly reactive and unstable in the presence of oxygen and water, and there are many other examples.

Moisture-sensitivity and degradation through water oxidation in air can be estimated

**Table S2:** Pourbaix hull stability at 0K.

mpid	Formula	$E_{pb}$ (eV/at.)	$V$ (V)	pH
mp-1500	BaS	0.966	-1	12
mp-1195594	Ba <sub>8</sub> Sn <sub>4</sub> S <sub>15</sub>	0.821	-0.7	10.18
mp-540689	$\beta$ -Ba <sub>2</sub> SnS <sub>4</sub>	0.834	-0.52	7.09
mp-12181	BaSnS <sub>2</sub>	0.697	-0.64	7.09
mp-1183370	BaSnS <sub>3</sub>	0.776	-0.52	6.91
mp-27802	BaSn <sub>2</sub> S <sub>3</sub>	0.582	-0.64	6.91
mp-2231	$\alpha$ -SnS	0.352	-0.64	6.73
mp-8781	SnS	0.398	-0.58	6.55

using  $E_{pb}$ , the Pourbaix stability against decomposition into both dissolved and solid phases (also called “energy above the Pourbaix hull” or “Pourbaix hull”).[4, 5] Singh et al. reported that a  $E_{pb} < 0.5$  eV/atom correlates favorably with stability,  $0.5$  eV/atom  $< E_{pb} < 1$  eV/atom may passivate, and  $E_{pb} > 1$  eV/atom are likely unstable.[5]

To explore moisture stability, we have assessed  $E_{pb}$  across the Ba-Sn-S compounds, and report the lowest values that occur across the entire Pourbaix diagram in Table S2. It is observed that none of the phases of interest are on the Pourbaix hull ( $E_{pb} = 0$  eV/atom), including binary end-points of BaS and SnS, but each has an  $E_{pb}$  less than 1 eV/atom (in the “metastable” regime, as defined by Singh et al.[5]). SnS is closest to the hull, and “stable” using the Singh cutoff.

Interestingly, when  $E_{pb}$  is computed at 1000K using the SISSO temperature-dependent free energy approach, as shown in Table S3, several phases now appear on the Pourbaix hull, including BaS, Ba<sub>8</sub>Sn<sub>4</sub>S<sub>15</sub>, and  $\beta$ -Ba<sub>2</sub>SnS<sub>4</sub> (all observed experimentally), while the other phases are considered “stable” using the Singh cutoff.

## S4. CHEMICAL POTENTIAL PHASE DIAGRAMS

### A. Sulfur chemical potential

Nitride phase diagrams are usually referenced to gaseous N<sub>2</sub>, as it is the lowest enthalpy state at 0K. However, it has been proposed that metastable nitrogen-rich nitrides could be

**Table S3:** Pourbaix hull stability at 1000K.

mpid	Formula	$E_{pb}$ (eV/at.)	$V$ (V)	pH
mp-1500	BaS	0	-2.52	9.82
mp-1195594	Ba <sub>8</sub> Sn <sub>4</sub> S <sub>15</sub>	0	-0.82	10.00
mp-540689	$\beta$ -Ba <sub>2</sub> SnS <sub>4</sub>	0	-0.52	8.18
mp-12181	BaSnS <sub>2</sub>	0.04	-1.06	9.82
mp-1183370	BaSnS <sub>3</sub>	0.035	-0.39	7.64
mp-27802	BaSn <sub>2</sub> S <sub>3</sub>	0.091	-1.06	9.82
mp-2231	$\alpha$ -SnS	0.219	-0.39	-2.00
mp-8781	SnS	0.147	-0.39	-2.00

synthesized by accessing nitrogen during synthesis in its “cracked” N reference state rather than lower enthalpy N<sub>2</sub>. [6] This is akin to increasing the chemical potential of nitrogen, and is possible because nitrogen can exist in multiple gaseous states. By “cracking” nitrogen gas at high temperatures, such an increase in chemical potential of nitrogen has been accessed by the Zakutayev group previously. This framework has been applied to both binary and ternary nitrides, [7, 8] but is more difficult to depict graphically due to the various tie-lines on ternary phase diagrams.

Similarly to nitrogen, sulfur can indeed exist in multiple gaseous states. Could metastable sulfur-rich phases also become accessible at increased chemical potential via a similar mechanism as in nitrides? Jackson and coworkers have shown that as temperature increases there is a phase change from the gaseous S<sub>8</sub> state to the S<sub>2</sub> state, which correlates to increased S chemical potential  $\Delta\mu_S$ . [9]

In Figure S4 we apply this analysis to a Materials Project (MP) phase diagram. On the MP database, the lowest enthalpy sulfur phase is S<sub>8</sub> (mp-96) as shown in (d), while the lowest energy S<sub>2</sub> phase (mp-1064933) as shown in (e) is  $\sim 350$  meV greater. Our GGA+U 0K phase diagram depicted in the manuscript is therefore referenced to the solid S<sub>8</sub> state, and is reproduced in (a). As a simple check of whether increased chemical potential could stabilize S-rich metastable states in Ba-Sn-S phase space, we recalculate the ternary phase diagram referenced to the solid S<sub>2</sub> state rather than S<sub>8</sub>. In this case, we find no instances of metastable S-rich phases that become stabilized across the ternary diagram, as shown

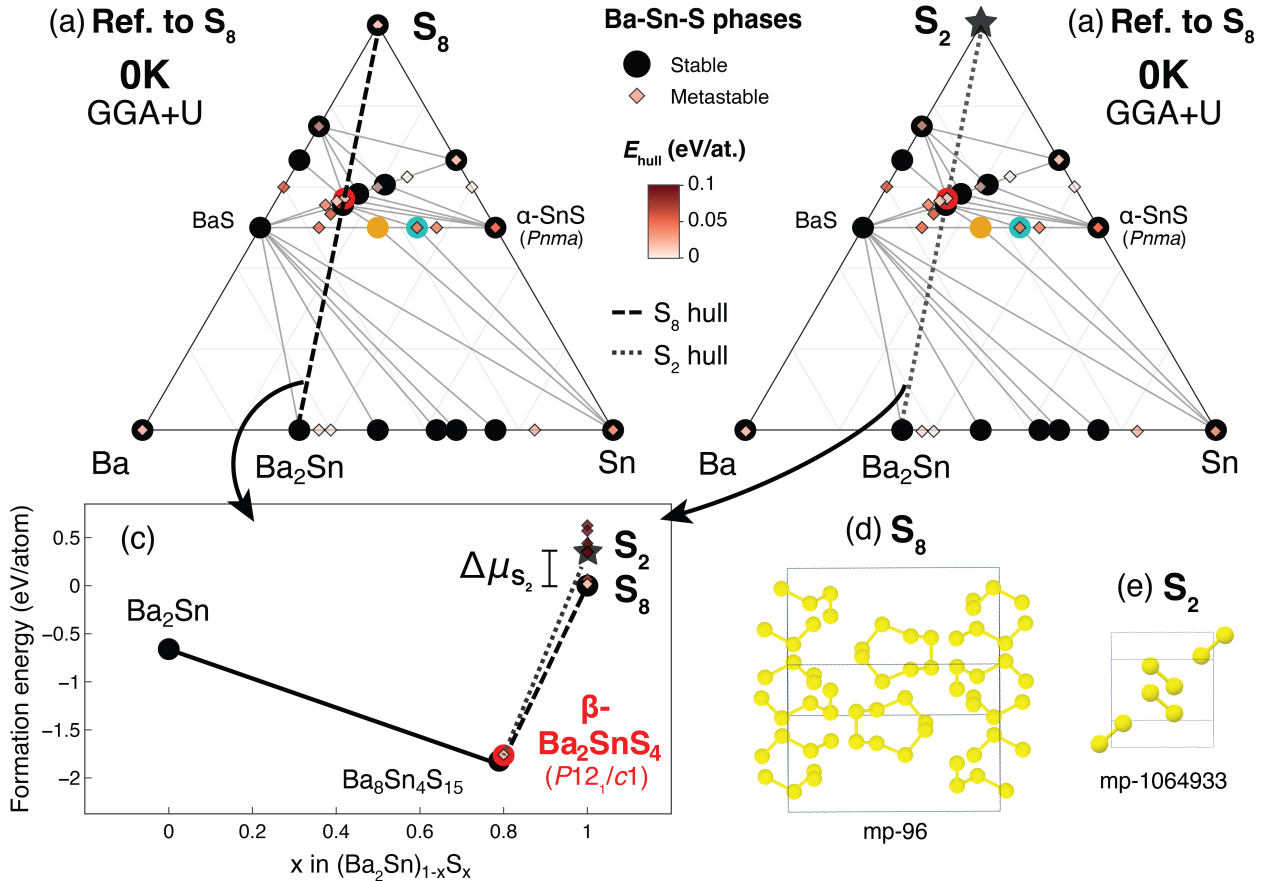


**Figure S4:** Phase diagrams referenced to (a) S<sub>8</sub> and to (b) S<sub>2</sub>. (c) An example tie-line on the phase diagram between Ba<sub>2</sub>Sn and S, with S<sub>8</sub> and S<sub>2</sub> hulls denoted. Crystal structure of (d) solid S<sub>8</sub> and (e) S<sub>2</sub>.

in (b). Analogous to the binary nitride example, panel (c) shows an example 2D phase diagram tie-line going from metal Ba<sub>2</sub>Sn to anion S, and through Ba<sub>2</sub>SnS<sub>4</sub> (note that the ternary “depth-of-hull” curvature is not depicted here, for simplicity[8]). The dashed line is the S<sub>8</sub> hull, and the dotted line is the new S<sub>2</sub> hull. It is observed there are no metastable phases that are stabilized between Ba<sub>2</sub>SnS<sub>4</sub> and S.

As an extreme example, we also increase the S chemical potential by a non-physical quantity (1 eV/atom), and in this case still no metastable phases are stabilized. We note that for compatibility solid phases of sulfur are referenced rather than gaseous, so this is just an approximation. Although this effect is not observed in Ba-Sn-S, this could be an interesting framework to apply to other sulfur-rich regions of metal sulfide phase spaces.

## B. Grand potential

Another way to depict the result of increasing sulfur chemical potential  $\Delta\mu_S$  is with ternary chemical potential phase diagrams. In Figure S5 we plot 3D chemical potential phase diagrams at 4 different temperatures, generated using `pymatgen` (and referenced to the ground state  $S_8$ ). As  $\Delta\mu_S$  increases ( $y$ -axis), S-rich phases become stable. As temperature increases (using the SISSO method), the chemical potential window at which the highlighted ternary phases are stable become more narrow. This is essentially another way of depicting the temperature-dependent ternary phase diagrams from the manuscript.

## Chemical potential phase diagrams

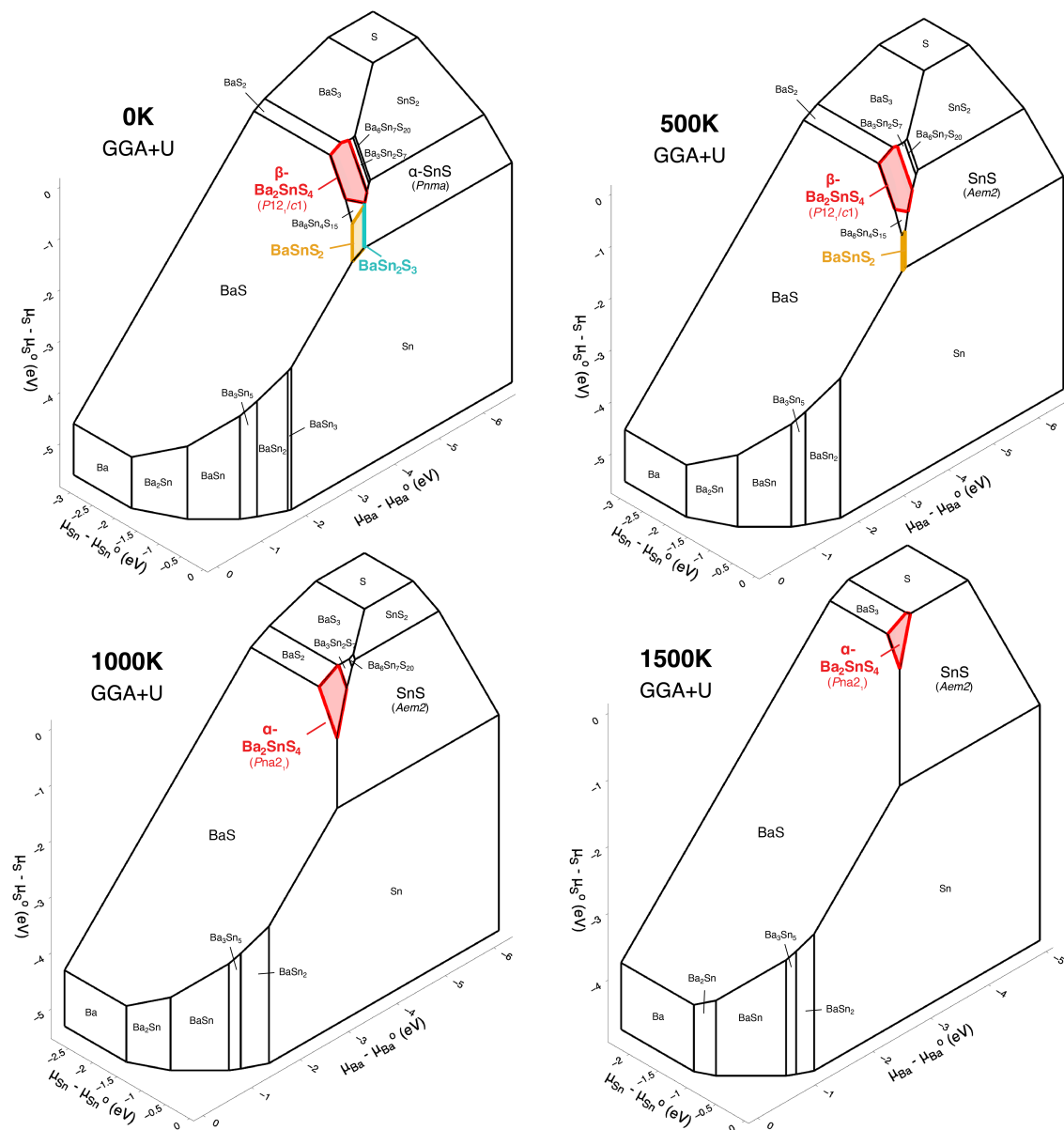


Figure S5: Chemical potential phase diagrams at 4 temperatures.

- [1] R. Kingsbury, A. S. Gupta, C. J. Bartel, J. M. Munro, S. Dwaraknath, M. Horton, and K. A. Persson, "Performance comparison of r 2 scan and scan metagga density functionals for solid materials via an automated, high-throughput computational workflow," *Physical Review Materials*,

- vol. 6, no. 1, p. 013801, 2022.
- [2] A. Wang, R. Kingsbury, M. McDermott, M. Horton, A. Jain, S. P. Ong, S. Dwaraknath, and K. A. Persson, “A framework for quantifying uncertainty in dft energy corrections,” *Scientific reports*, vol. 11, no. 1, p. 15496, 2021.
- [3] C. J. Bartel, S. L. Millican, A. M. Deml, J. R. Rumpitz, W. Tumas, A. W. Weimer, S. Lany, V. Stevanović, C. B. Musgrave, and A. M. Holder, “Physical descriptor for the gibbs energy of inorganic crystalline solids and temperature-dependent materials chemistry,” *Nature communications*, vol. 9, no. 1, pp. 1–10, 2018.
- [4] K. A. Persson, B. Waldwick, P. Lazic, and G. Ceder, “Prediction of solid-aqueous equilibria: Scheme to combine first-principles calculations of solids with experimental aqueous states,” vol. 85, no. 23, p. 235438.
- [5] A. K. Singh, L. Zhou, A. Shinde, S. K. Suram, J. H. Montoya, D. Winston, J. M. Gregoire, and K. A. Persson, “Electrochemical stability of metastable materials,” vol. 29, pp. 10159–10167.
- [6] A. Zakutayev, “Design of nitride semiconductors for solar energy conversion,” *Journal of Materials Chemistry A*, vol. 4, no. 18, pp. 6742–6754, 2016.
- [7] W. Sun, A. Holder, B. Orvañanos, E. Arca, A. Zakutayev, S. Lany, and G. Ceder, “Thermodynamic routes to novel metastable nitrogen-rich nitrides,” *Chemistry of Materials*, vol. 29, no. 16, pp. 6936–6946, 2017.
- [8] W. Sun, C. J. Bartel, E. Arca, S. R. Bauers, B. Matthews, B. Orvañanos, B.-R. Chen, M. F. Toney, L. T. Schelhas, W. Tumas, *et al.*, “A map of the inorganic ternary metal nitrides,” *Nature materials*, vol. 18, no. 7, pp. 732–739, 2019.
- [9] A. J. Jackson, D. Tiana, and A. Walsh, “A universal chemical potential for sulfur vapours,” *Chemical science*, vol. 7, no. 2, pp. 1082–1092, 2016.